Observation of Quantum Interference in the Plasmonic Hong-Ou-Mandel Effect

G. Di Martino,[1] Y. Sonnefraud,[1,2] M. S. Tame,[1,3,*] S. Kéna-Cohen,[1,4] F. Dieleman,[1] Ş. K. Özdemir,[5] M. S. Kim,[6] and S. A. Maier[1,†]

[1]*Experimental Solid State Group, Imperial College London, Blackett Laboratory, SW7 2AZ London, United Kingdom*

[2]*Institut Néel, CNRS UPR2940, 25 rue des Martyrs, 38042 Grenoble, France*

[3]*University of KwaZulu-Natal, School of Chemistry and Physics, 4001 Durban, South Africa*

[4]*Department of Engineering Physics, École Polytechnique de Montréal, C.P. 6079 succursale Centre-ville, Montréal, Québec H3C 3A7, Canada*

[5]*Department of Electrical and Systems Engineering, Washington University, St. Louis, Missouri 63130, USA*

[6]*Quantum Optics and Laser Science Group, Imperial College London, Blackett Laboratory, SW7 2AZ London, United Kingdom*

(Received 30 January 2014; published 15 April 2014)

Surface plasmon polaritons (SPPs) are electromagnetic excitations coupled to electron-charge density waves at metal-dielectric interfaces. They have recently been found to enable a range of nanophotonic devices for controlling systems at the quantum level, including single-photon sources, transistors, and ultracompact quantum circuitry. An important quantum feature of SPPs yet to be fully explored is their bosonic nature. In this work, we report direct evidence of the bosonic nature of SPPs in a scattering-based beam splitter. A parametric down-conversion source is used to produce two indistinguishable photons, each of which is converted into a SPP on a metal-stripe waveguide and then made to interact through a semitransparent Bragg mirror. In this plasmonic analog of the Hong-Ou-Mandel experiment, we measure a coincidence dip with a visibility of 72%, a key signature that SPPs are bosons and that quantum interference is clearly involved. Our work opens up possibilities for the study of fundamental quantum effects in plasmonic systems and their related applications.

DOI: 10.1103/PhysRevApplied.1.034004

Nanophotonic systems based on plasmonic components are currently attracting considerable attention due to the ways in which the electromagnetic field can be localized and controlled [1,2]. In the classical regime, a wide range of applications are being pursued, including nanoimaging [3], biosensing [4], and solar cells [5]. Recently, researchers have started to investigate plasmonics in the quantum regime [6]. Devices have been proposed for a variety of applications in quantum information science [6–9]. Despite the remarkable progress made so far, there are many fundamental aspects of quantum plasmonic systems that remain unexplored. One key property is the bosonic nature of single surface plasmon polaritons (SPPs). The quasiparticle nature of SPPs, consisting of a photon coupled to a density wave of electrons, makes them an unusual type of excitation. While it is generally accepted that in theory SPPs are bosons, as of yet, the quantum statistical behavior of SPPs has not been clearly demonstrated experimentally. The bosonic nature of *photons* was explicitly verified in the seminal experiment of Hong, Ou, and Mandel [10]. Recent work using plasmonic waveguides has hinted that SPPs are bosons by observing the preservation of properties of the photons used to excite them [11–14] and the Hong-Ou-Mandel (HOM) effect, both indirectly by using a photonic beam splitter [15] and directly by using a plasmonic beam splitter [16]. However, the question as to whether quantum interference is involved remains open due to the low HOM contrast observed, which can be obtained via classical interference of light [17–21]. In order to verify the bosonic nature of single excitations in the quantum regime, it is vital to observe quantum interference [17–19].

In this work, we report the observation of quantum interference in the HOM effect for SPPs. We use spontaneous parametric down-conversion (SPDC) to produce two indistinguishable photons [22,23], each of which is converted into a SPP on separate metal-stripe waveguides [24–26]. This approach alleviates difficulties related to indistinguishability when using quantum emitters as single-SPP sources [27–29]. The generated SPPs interact on a beam splitter via a scattering process [30–32], and we find that they exhibit the distinct bunching effect expected for bosons, with the results clearly showing that quantum interference is involved.

Experimental setup.—The setup used to conduct our investigation is shown in Fig. 1(a). Here, photon pairs are generated at a wavelength of 808 nm by using a 100-mW continuous wave laser ($\lambda = 404$ nm) focused onto a beta barium borate (BBO) crystal cut for type-I SPDC [22]. Phase-matching conditions lead to the photons from a given

*markstame@gmail.com
†s.maier@imperial.ac.uk

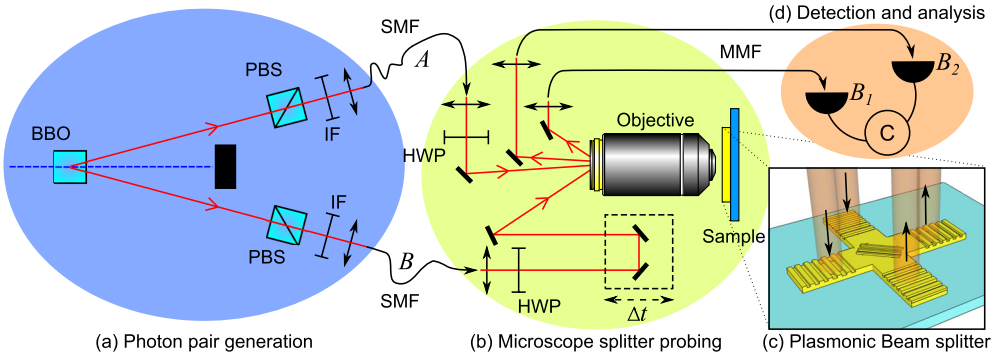

FIG. 1. Experimental setup. (a) Photon pair generation. Photon pairs are generated via spontaneous parametric down-conversion by using a pump laser focused onto a BBO crystal and filtered by using interference filters (IFs). Each photon is coupled into a single-mode fiber (SMF). (b) Microscopy. The photons from the SMFs are collimated and half-wave plates (HWPs) are used to optimize SPP excitation. A time delay is introduced on one path. (c) Plasmonic beam splitter. The photons are focused onto separate spots on the input gratings by using a microscope objective. The beams at the output gratings are collected and coupled into multimode fibers (MMFs). (d) Detection and analysis. The outputs of the MMFs are sent to avalanche photodiodes B_1 and B_2, where coincident detection events are measured.

pair being emitted into antipodal points of a cone with an opening angle of 6° [23]. Figure 1(a) shows that the antipodal points chosen are in plane. Polarizing beam splitters (PBSs) in the paths of the down-converted beams remove any parasitic light with the incorrect polarization. IFs with a central wavelength of 800 nm and a 22-nm bandwidth are placed in both paths to spectrally select out the down-converted photons. The photons are injected into SMFs. After collimation of the output from the fibers, the polarization is adjusted by using HWPs to maximize the excitation of SPPs on the sample. The polarization dependence of the SPP excitation efficiency is the same as in Ref. [26]. In order to control how well the SPPs generated from the photons interfere with each other, we introduce a degree of distinguishability. Their spatial and spectral characteristics are closely matched by the SMFs and IFs, so a time delay is introduced in one path by using a motorized delay line of distance d. This distance provides a variable delay of $\Delta t = d/c$ between the single-photon wave packets, so that the arrival time of the SPPs at the plasmonic beam splitter can be controlled and a degree of distinguishability introduced. The photons are focused onto separate gratings (spot size 2 μm) at the inputs of an X-shaped plasmonic beam splitter, shown in Fig. 1(c), by a microscope objective (100×, NA 0.8) and converted into SPPs due to phase-matching conditions [26,33]. The SPPs propagate along the waveguides, passing through the central body of the beam splitter where they interfere via a scattering process. After scattering, they reach the output gratings and are converted back into light. Figure 2(c) shows the SPP intensity from the two output gratings. MMFs collect this outcoupled light, directing it to silicon avalanche photodiode (APD) detectors B_1 and B_2, which monitor the arrival of the photons. Detection events are time tagged (PicoQuant Hydraharp 400), coincidences are evaluated within a $t_c = 2$ ns time window, and reported error bars correspond to standard deviations.

Beam splitter characterization.—The plasmonic beam splitter consists of two 2-μm-wide, 70-nm-thick gold stripe waveguides that cross at a right angle at their midpoint, as shown in Fig. 2(a). These waveguides support a single low-loss leaky SPP mode [25] and a number of short-range bound modes [24]. The beam splitter structure is defined on a glass substrate by electron beam lithography (EBL). A second EBL step is used to overlay 90-nm-thick input and output gratings and central scattering elements, as described in Ref. [34]. The grating periodicity $g = 620$ nm is chosen to couple effectively to the low-loss SPP mode. The SPP propagation length (the length at which the intensity decreases to $1/e$ of its original value) is $l = 12.4 \pm 0.3\,\mu$m. This value has been measured on gold stripe waveguides of increasing length, as described in Ref. [26] and shown in Fig. 2(b). The distance between incoupling and outcoupling gratings is $L = 12.5\ \mu$m.

In the beam splitter, the splitting operation is obtained via a scattering process, in direct contrast to previous studies using coupled waveguides [16]. The scattering element is a semitransparent Bragg reflector, consisting of three ridges spaced by a distance $p = 500$ nm, deposited on the central part of the beam splitter, as shown in Fig. 2(a). Bragg reflectors such as the one we use have been studied extensively in the literature, mostly as effective mirrors in the one-dimensional case of normal incidence, both on an infinite interface and on plasmonic waveguides [31]. Some reflectors have also been studied in the two-dimensional case with different structures, such as a grating made of nanoparticles [30,35], or with ridges on an infinite interface [32]. We have chosen this Bragg reflector approach over coupled waveguides due to its compactness and the potential for multiple elements to be integrated: The

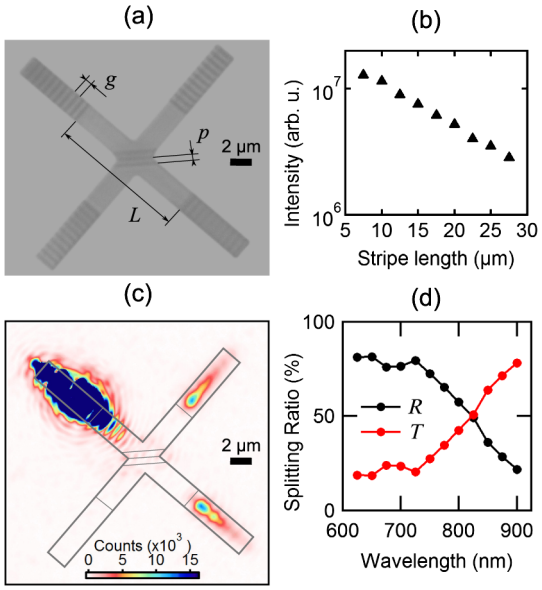

FIG. 2. Plasmonic beam splitter. (a) Optical image of the beam splitter. The in and out gratings consist of 11 ridges, each being repeated at an increment of $g = 620$ nm from the waveguide end. The distance between gratings is $L = 12.5$ μm. The Bragg reflector is made out of three ridges with a center-to-center distance of $p = 500$ nm. (b) Intensity outcoupled from a single waveguide as a function of length when excited by a laser at 808 nm by using the method in Ref. [26]. (c) Optical image of the splitter when the SPPs are excited by a laser at 808 nm focused on the top-left grating. Light is outcoupled at the top right and bottom right with almost identical intensity. The integration time is adjusted to give a reasonable contrast for the output, leading to a saturation at the input caused by the scattered field. (d) Transmission T and reflection R as a function of wavelength.

zone over which the SPPs interact represents less than two wavelengths.

To obtain the wavelength dependence of the transmission and reflection T and R, respectively, of the Bragg element, we use light from a supercontinuum filtered to the appropriate wavelength and focused on one of the input gratings, e.g., the top-left grating, as shown in Fig. 2(c). For each wavelength, the intensity is integrated over the complete area of each output grating [top-right and bottom-right gratings in Fig. 2(c)]. The value of T is the ratio between the intensity at the output grating directly opposite the input grating and the total intensity at both output gratings. While this method does not account for loss due to radiative scattering at the Bragg reflector or during SPP propagation, it gives the relative transmission T of the beam splitter. From the above, the relative reflection coefficient is then $R = 1 - T$. In order to maximize quantum interference in the HOM effect, the beam splitter must have $R = T = 1/2$ [10]. We check the splitting ratio for a range of wavelengths for optimal splitting. As shown in Fig. 2(d), a Bragg reflector with ridges having a period of 500 nm gives $T = 0.49 \pm 0.05$ for incident SPPs at $\lambda_0 = 808$ nm—the wavelength of the photons used in our experiment. The value of T remains the same for every input of the beam splitter.

Theoretical background.—In the HOM experiment, due to phase-matching conditions of the SPDC process, a single photon in path i is well approximated by the quantum state $|1\rangle_i = \int d\omega_i \phi_i(\omega_i) \hat{a}_i^\dagger(\omega_i)|0\rangle$ [10,23], where $\phi_i(\omega_i)$ is a normalized spectral amplitude of the photon, $|0\rangle$ is the vacuum state, and $\hat{a}_i^\dagger(\omega_i)$ is a creation operator, which together with the operator $\hat{a}_i(\omega_i)$ satisfies the bosonic commutation relation $[\hat{a}_i(\omega_i), \hat{a}_i^\dagger(\omega_i')] = \delta(\omega_i - \omega_i')$ [36]. Taking the input state at the beam splitter as $|1\rangle_A|1\rangle_B$ and applying the unitary transformations $\hat{a}_A^\dagger(\omega) = i\sqrt{R}\hat{a}_{B_1}^\dagger(\omega) + \sqrt{T}\hat{a}_{B_2}^\dagger(\omega)$ and $\hat{a}_B^\dagger(\omega) = \sqrt{T}\hat{a}_{B_1}^\dagger(\omega) + i\sqrt{R}\hat{a}_{B_2}^\dagger(\omega)$ leads to the output state

$$\eta_{\text{in}}\eta_{\text{out}}[i\sqrt{R}\sqrt{T}|2\rangle_{B_1}|0\rangle_{B_2} + i\sqrt{R}\sqrt{T}|0\rangle_{B_1}|2\rangle_{B_2} - R|1\rangle_{B_1}|1\rangle_{B_2} + T|1\rangle_{B_1}|1\rangle_{B_2}], \quad (1)$$

where η_{in} (η_{out}) accounts for loss in the input (output) arms of the beam splitter [36]. In the ideal case, $R = T = 1/2$ and the terms with one excitation in each output interfere destructively. This interference can be seen only in the quantum regime and leads to the output state

$$|1\rangle_A|1\rangle_B \rightarrow \frac{1}{\sqrt{2}}(|2\rangle_{B_1}|0\rangle_{B_2} + |0\rangle_{B_1}|2\rangle_{B_2}). \quad (2)$$

Thus, the photons display bosonic behavior by bunching together. This bunching occurs regardless of the loss at the input and output stages, which only reduces the rate at which the process occurs. From Eq. (2), the probability of detecting a coincidence event where a photon is present at each output drops to zero when the photons interfere. On the other hand, when they are unable to interfere, e.g., due to their arrival time, each output state in Eq. (1) occurs with equal probability, and the probability of detecting a coincidence is 1/2 [scaled by $(\eta_{\text{in}}\eta_{\text{out}})^2$]. In the time domain, when $R = T = 1/2$, Eq. (1) leads to a coincidence probability $P(\Delta t) = (\eta_{\text{in}}\eta_{\text{out}})^2[1 - \text{sinc}^2(\Delta t \cdot \Delta\omega/2)]/2$. Here, Δt is the delay between the photons, and top-hat amplitudes $\phi_i(\omega_i)$ are used with a FWHM of $\Delta\omega$. Thus, we have $P(0) = 0$ and $P(\Delta t \gg \tau_c) = (\eta_{\text{in}}\eta_{\text{out}})^2/2$, where $\tau_c \sim 2\pi/\Delta\omega$ is the photon coherence time and $\tau_c \ll t_c$, with t_c the coincidence window of the detection events.

Quantum interference.—We first confirm that the photons generated by our source exhibit the above-described HOM effect in a conventional beam splitter. For this confirmation, we measured the output coincidences, as a function of time delay between the arrival of the input photons. At zero delay the coincidence rate drops to a minimum value N_{min} as expected. This drop is quantified by using the visibility $V_P = (N_{\text{max}} - N_{\text{min}})/N_{\text{max}}$ [17,19],

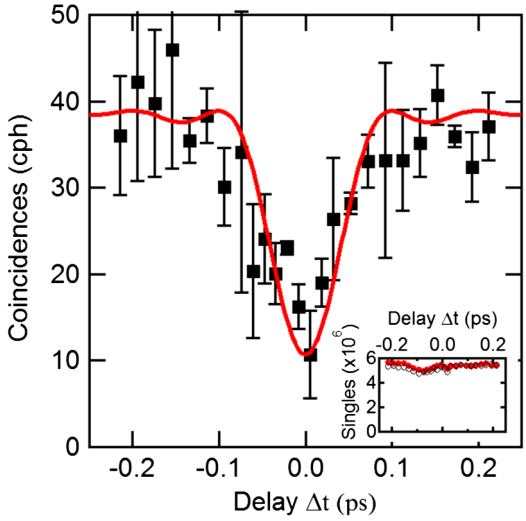

FIG. 3. Plasmonic Hong-Ou-Mandel dip. Black squares: Coincidence rate as a function of time delay Δt. The red curve is a theoretical fit, $N(\Delta t)$, based on the coincidence probability $P(\Delta t)$ corrected for accidentals [38]. From the theory fit, we extract a coherence time for the SPPs of approximately 0.1 ps, which is consistent with the coherence time obtained from the measured photonic dip. This result confirms that during the photon-SPP conversion process the coherence properties of the single-photon wave packets and the single SPPs are similar and that the wave packet has not been significantly altered by the conversion process or propagation. The inset shows the singles rates (in counts/h) as a function of Δt: red disks for detector B_1 and black circles for B_2. The visibility obtained from the plasmonic dip is $V_{\mathrm{SPP}} = 0.72 \pm 0.13$.

where $N_{\max}$ is the maximum value of coincidences far from the dip center. We find $V_P = 0.67 \pm 0.05$. This value is limited by a number of factors, including the bandwidth of the IFs used in our experiment, the resolution of the time delay, the spatial mismatch between the modes of the photons at the beam splitter, and the deviation of the beam splitter from the ideal case ($R = T = 0.5$). Despite these factors, with a visibility larger than 0.5 we can confirm that the drop is due to *quantum* interference [17–19].

We then probe the plasmonic beam splitter, as depicted in Fig. 1. When the coupling of single photons into the SPP waveguides is optimized, the count rate due to SPPs scattered by the output grating and detected by APD $B_{1,2}$ is $N_{B_{1,2}} \sim 5.5 \times 10^6$ counts per hour (counts/h), as shown in the inset in Fig. 3. The time-resolved correlation data show an average number of coincidences of 54.8 ± 1.4 counts/h far from zero time delay and 30.2 ± 2.4 counts/h at zero delay. A proportion of these counts are due to accidental coincidences from uncorrelated photon pairs which couple into the beam splitter but do not correspond to true correlated pairs from the source; thus, we subtract them from the overall counts. We measure the contribution of coincidences due to the accidentals by introducing an electronic time delay between the events at both detectors larger than the coincidence window, thus capturing the coincidence counts from uncorrelated pairs. The accidental coincidence count far from zero delay is 15.4 ± 2.2, so that the average coincidence rate is then 39.4 ± 0.9 counts/h, as shown in Fig. 3. On the other hand, at zero delay we have an accidental rate of 19.5 ± 2.2 giving a coincidence rate of 10.7 ± 5.1 counts/h at zero delay, which leads to a visibility for the plasmonic HOM dip of $V_{\mathrm{SPP}} = 0.72 \pm 0.13$. The observed dip confirms that single SPPs bunch together as bosons, and as the visibility is larger than 0.5 this result confirms that quantum interference is involved in the bunching process [17–19]. The plasmonic visibility is again limited by a number of factors, including the bandwidth of the IFs and the time-delay resolution. The use of a narrower bandwidth is possible, giving photons with improved spectral definition for interference; however, this definition comes at the expense of longer data collection times, where the data become sensitive to the coupling stability of the setup. The resolution of the time delay is limited by the accuracy of the translation stage, with shorter step sizes allowing for improved accuracy near the dip minimum. One reason for the improved visibility compared to the photonic case may be due to the integrated waveguide providing better spatial overlap of the modes at the beam splitter [37]. Furthermore, any loss due to radiative scattering at the beam splitter (measured as $< 10\%$) occurs instantaneously and can be included within η_{out}, which does not play a role in reducing the visibility [20]. Finally, note that, when the coincidence rate drops as the single SPPs interfere, the count rate at each APD remains unchanged, as shown in Fig. 3. This effect is due to the small portion of *pairs* of single excitations (compared to the total) that survive the process of propagation, splitting and outcoupling: In most cases, at least one excitation from a pair will be lost. Therefore, the count rate at each APD allows the efficiency of the system to be monitored to ensure that the dip is not caused by loss fluctuations.

Summary.—In this work, we experimentally investigate a key quantum feature of SPPs, that is, their bosonic nature. We use single photons generated via parametric down-conversion to excite single SPPs on a metallic stripe beam splitter. The SPPs interact via a scattering process, and we directly observe the HOM effect. Here, the SPPs show a distinct bunching behavior as expected for bosons, with the results clearly showing that quantum interference is involved. Our investigation confirms the bosonic nature of single SPPs in the quantum regime, and, by doing so, it opens up exciting opportunities for controlling quantum states of light in ultracompact nanophotonic plasmonic circuitry.

This work was supported by the United Kingdom Engineering and Physical Sciences Research Council, the Leverhulme Trust, the European Office of Aerospace Research and Development (EOARD), and the Qatar

National Research Fund (Grant No. NPRP 4-554-1-084). We thank P. L. Knight, R. Oulton, and A. Lupi for comments and discussions. S. K. O. thanks L. Yang and F. Nori for support.

[1] D. K. Gramotnev and S. I. Bozhevolnyi, Plasmonics beyond the diffraction limit, Nat. Photonics **4**, 83 (2010).
[2] V. Giannini, A. I. Fernández-Domínguez, Y. Sonnefraud, T. Roschuk, R. Fernández-Garca, and S. A. Maier, Controlling light localization and light-matter interactions with nanoplasmonics, Small **6**, 2498 (2010).
[3] S. Kawata, Y. Inouye, and P. Verma, Plasmonics for near-field nano-imaging and superlensing, Nat. Photonics **3**, 388 (2009).
[4] J. N. Anker, W. P. Hall, O. Lyandres, N. C. Shah, J. Zhao, and R. P. Van Duyne, Biosensing with plasmonic nanosensors, Nat. Mater. **7**, 442 (2008).
[5] H. A. Atwater and A. Polman, Plasmonics for improved photovoltaic devices, Nat. Mater. **9**, 205 (2010).
[6] M. S. Tame, K. R. McEnery, Ş. K. Özdemir, J. Lee, S. A. Maier, and M. S. Kim, Quantum plasmonics, Nat. Phys. **9**, 329 (2013).
[7] A. V. Akimov, A. Mukherjee, C. L. Yu, D. E. Chang, A. S. Zibrov, P. R. Hemmer, H. Park, and M. D. Lukin, Generation of single optical plasmons in metallic nanowires coupled to quantum dots, Nature (London) **450**, 402 (2007).
[8] D. E. Chang, A. S. Sø rensen, E. A. Demler, and M. D. Lukin, A single-photon transistor using nanoscale surface plasmons, Nat. Phys. **3**, 807 (2007).
[9] N. P. de Leon, M. D. Lukin, and H. Park, Quantum plasmonic circuits, IEEE J. Sel. Top. Quantum Electron. **18**, 1781 (2012).
[10] C. K. Hong, Z. Y. Ou, and L. Mandel, Measurement of subpicosecond time intervals between two photons by interference, Phys. Rev. Lett. **59**, 2044 (1987).
[11] E. Altewischer, M. P. van Exter, and J. P. Woerdman, Plasmon-assisted transmission of entangled photons, Nature (London) **418**, 304 (2002).
[12] S. Fasel, F. Robin, E. Moreno, D. Erni, N. Gisin, and H. Zbinden, Energy-time entanglement preservation in plasmon-assisted light transmission, Phys. Rev. Lett. **94**, 110501 (2005).
[13] S. Fasel, M. Halder, N. Gisin, and H. Zbinden, Quantum superposition and entanglement of mesoscopic plasmons, New J. Phys. **8**, 13 (2006).
[14] A. Huck, S. Smolka, P. Lodahl, A. S. Srensen, A. Boltasseva, J. Janousek, and U. L. Andersen, Demonstration of quadrature-squeezed surface plasmons in a gold waveguide, Phys. Rev. Lett. **102**, 246802 (2009).
[15] G. Fujii, T. Segawa, S. Mori, N. Namekata, D. Fukuda, and S. Inoue, Preservation of photon indistinguishability after transmission through surface-plasmon-polariton waveguide, Opt. Lett. **37**, 1535 (2012).
[16] R. W. Heeres, L. P. Kouwenhoven, and V. Zwiller, Quantum interference in plasmonic circuits, Nat. Nanotechnol. **8**, 719–722 (2013).
[17] J. G. Rarity, P. R. Tapster, and R. Loudon, Non-classical interference between independent sources, J. Opt. B **7**, S171 (2005).
[18] L. Mandel, Quantum effects in one-photon and two-photon interference, Rev. Mod. Phys. **71**, S274 (1999).
[19] R. Ghosh and L. Mandel, Observation of nonclassical effects in the interference of two photons, Phys. Rev. Lett. **59**, 1903 (1987).
[20] D. Ballester, M. S. Tame, and M. S. Kim, Quantum theory of surface plasmon polariton scattering, Phys. Rev. A **82**, 012325 (2010).
[21] Y.-S. Kim, O. Slattery, P. S. Kuo, and X. Tang, Two-photon interference with continuous-wave multi-mode coherent light, Opt. Express **22**, 3611 (2014).
[22] D. C. Burnham and D. L. Weinberg, Observation of simultaneity in parametric production of optical photon pairs, Phys. Rev. Lett. **25**, 84 (1970).
[23] C. K. Hong and L. Mandel, Experimental realization of a localized one-photon state, Phys. Rev. Lett. **56**, 58 (1986).
[24] B. Lamprecht, J. R. Krenn, G. Schider, H. Ditlbacher, M. Salerno, N. Felidj, A. Leitner, F. R. Aussenegg, and J.-C. Weeber, Surface plasmon propagation in microscale metal stripes, Appl. Phys. Lett. **79**, 51 (2001).
[25] R. Zia, M. D. Selker, and M. L. Brongersma, Leaky and bound modes of surface plasmon waveguides, Phys. Rev. B **71**, 165431 (2005).
[26] G. Di Martino, Y. Sonnefraud, S. Kéna-Cohen, M. S. Tame, Ş. K. Özdemir, M. S. Kim, and S. A. Maier, Quantum statistics of surface plasmon polaritons in metallic stripe waveguides, Nano Lett. **12**, 2504 (2012).
[27] R. Kolesov, B. Grotz, G. Balasubramanian, R. J. Sthr, A. A. L. Nicolet, P. R. Hemmer, F. Jelezko, and J. Wrachtrup, Wave-particle duality of single surface plasmon polaritons, Nat. Phys. **5**, 470 (2009).
[28] A. Cuche, O. Mollet, A. Drezet, and S. Huant, "Deterministic" quantum plasmonics, Nano Lett. **10**, 4566 (2010).
[29] O. Mollet, S. Huant, G. Dantelle, T. Gacoin, and A. Drezet, Quantum plasmonics: Second-order coherence of surface plasmons launched by quantum emitters into a metallic film, Phys. Rev. B **86**, 045401 (2012).
[30] H. Ditlbacher, J. R. Krenn, G. Schider, A. Leitner, and F. R. Aussenegg, Two-dimensional optics with surface plasmon polaritons, Appl. Phys. Lett. **81**, 1762 (2002).
[31] J.-C. Weeber, M. U. González, A.-L. Baudrion, and A. Dereux, Surface plasmon routing along right angle bent metal strips, Appl. Phys. Lett. **87**, 221101 (2005).
[32] M. U. González, J.-C. Weeber, A.-L. Baudrion, A. Dereux, A. L. Stepanov, J. R. Krenn, E. Devaux, and T. W. Ebbesen, Design, near-field characterization, and modeling of surface-plasmon Bragg mirrors, Phys. Rev. B **73**, 155416 (2006).
[33] M. S. Tame, C. Lee, J. Lee, D. Ballester, M. Paternostro, A. V. Zayats, and M. S. Kim, Single-photon excitation of surface plasmon polaritons, Phys. Rev. Lett. **101**, 190504 (2008).
[34] S. Kéna-Cohen, P. N. Stavrinou, D. D. C. Bradley, and S. A. Maier, Confined surface plasmon-polariton amplifiers, Nano Lett. **13**, 1323 (2013).
[35] M. Quinten, A. Leitner, J. R. Krenn, and F. R. Aussenegg, Electromagnetic energy transport via linear chains of silver nanoparticles, Opt. Lett. **23**, 1331 (1998).

[36] R. Loudon, *The Quantum Theory of Light* (Oxford University, Oxford, 2000), 3rd ed.

[37] A. Politi, M. J. Cryan, J. G. Rarity, S. Yu, and J. L. O'Brien, Silica-on-silicon waveguide quantum circuits, Science **320**, 646 (2008).

[38] The coincidence rate is $N(\Delta t) = N_t P(\Delta t)$, where N_t is the rate of true correlated pairs from the source. The value of $N_t(\eta_{\text{in}}\eta_{\text{out}})^2/2$ in the expression for $N(\Delta t)$ is obtained by measuring $N^{\text{exp}}(\Delta t \gg \tau_c)$. Here, there is a contribution from uncorrelated pairs, N_{acc}, which arrive at the APDs within the coincidence time $t_c = 2$ ns. Thus, $N^{\text{exp}}(\Delta t \gg \tau_c) = N_t(\eta_{\text{in}}\eta_{\text{out}})^2/2 + N_{\text{acc}}$. A large proportion of N_{acc} are measured directly with the remainder given by $N^r_{\text{acc}} = N_{\text{acc}} - N^m_{\text{acc}}$. This relation leads to $N(\Delta t) = N^r_{\text{acc}} + [N^{\text{exp}}(\Delta t \gg \tau_c) - N_{\text{acc}}][1 - \text{sinc}^2(\Delta t \cdot \Delta\omega/2)]$, where we have $N^r_{\text{acc}} = N^{\text{exp}}(0) - N^m_{\text{acc}}$.